BIOCHEMISTRY
including biophysical chemistry & molecular biology

Article

pubs.acs.org/biochemistry

Dynamics of an Active-Site Flap Contributes to Catalysis in a JAMM Family Metallo Deubiquitinase

Amy N. Bueno,[†,#] Rashmi K. Shrestha,[†,#] Judith A. Ronau,[†,‡] Aditya Babar,[†] Michael J. Sheedlo,[†] Julian E. Fuchs,[§,∥] Lake N. Paul,[⊥] and Chittaranjan Das*[,†]

[†]Department of Chemistry, Purdue University, 560 Oval Drive, West Lafayette, Indiana 47907, United States
[§]Centre for Molecular Informatics, Department of Chemistry, University of Cambridge, Cambridge CB2 1EW, United Kingdom
[⊥]Bindley Biosciences Center, Purdue University, West Lafayette, Indiana 47907, United States

Supporting Information

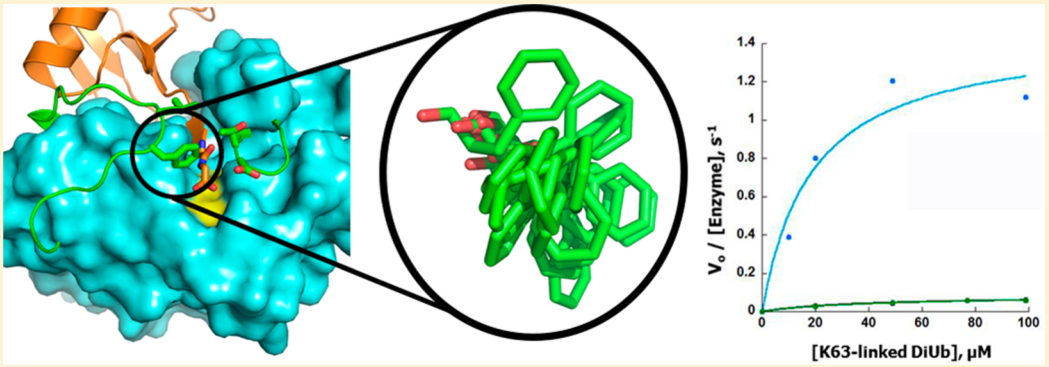

ABSTRACT: The endosome-associated deubiquitinase (DUB) AMSH is a member of the JAMM family of zinc-dependent metallo isopeptidases with high selectivity for Lys63-linked polyubiquitin chains, which play a key role in endosomal−lysosomal sorting of activated cell surface receptors. The catalytic domain of the enzyme features a flexible flap near the active site that opens and closes during its catalytic cycle. Structural analysis of its homologues, AMSH-LP (AMSH-like protein) and the fission yeast counterpart, Sst2, suggests that a conserved Phe residue in the flap may be critical for substrate binding and/or catalysis. To gain insight into the contribution of this flap in substrate recognition and catalysis, we generated mutants of Sst2 and characterized them using a combination of enzyme kinetics, X-ray crystallography, molecular dynamics simulations, and isothermal titration calorimetry (ITC). Our analysis shows that the Phe residue in the flap contributes key interactions during the rate-limiting step but not to substrate binding, since mutants of Phe403 exhibit a defect only in k_{cat} but not in K_M. Moreover, ITC studies show Phe403 mutants have similar K_D for ubiquitin compared to the wild-type enzyme. The X-ray structures of both Phe403Ala and the Phe403Trp, in both the free and ubiquitin bound form, reveal no appreciable structural change that might impair substrate or alter product binding. We observed that the side chain of the Trp residue is oriented identically with respect to the isopeptide moiety of the substrate as the Phe residue in the wild-type enzyme, so the loss of activity seen in this mutant cannot be explained by the absence of a group with the ability to provide van der Waals interactions that facilitate the hyrdolysis of the Lys63-linked diubiquitin. Molecular dynamics simulations indicate that the flap in the Trp mutant is quite flexible, allowing almost free rotation of the indole side chain. Therefore, it is possible that these different dynamic properties of the flap in the Trp mutant, compared to the wild-type enzyme, manifest as a defect in interactions that facilitate the rate-limiting step. Consistent with this notion, the Trp mutant was able to cleave Lys48-linked and Lys11-linked diubiquitin better than the wild-type enzyme, indicating altered mobility and hence reduced selectivity.

Ubiquitination, covalent attachment of the 76-amino-acid protein ubiquitin to target proteins via formation of an isopeptide bond between the side chain of the amino group of a lysine residue of the target and the terminal carboxylate group (Gly76) of ubiquitin, has emerged as an important form of protein posttranslational modification that rivals phosphorylation in scope and complexity.[1−5] This protein modification, catalyzed by the sequential action of three enzymatic systems, E1 (ubiquitin activating enzyme), E2 (ubiquitin conjugating enzyme), and E3 (ubiquitin ligase), usually results in the attachment of polyubiquitin chains to target proteins via successive addition of subsequent ubiquitin groups in a chain-like manner, emanating from the first ubiquitin directly appended to the target.[6−9] In the case of homotypic chains, the linking pattern involves a specific amino group of an internal ubiquitin, either the ε-amino group of one of

Received: June 9, 2015
Revised: September 13, 2015
Published: September 14, 2015

DOI: 10.1021/acs.biochem.5b00631
Biochemistry 2015, 54, 6038−6051

ubiquitin's seven Lys residues or its N-terminal amino group (Met1), linked to the carboxylate group of Gly76 of a succeeding monomer in a repetitive fashion. The eight distinct linkage isomers of such homotypic polyubiquitin chains are characterized by a distinct three-dimensional architecture, which gives rise to distinct biological outcomes for proteins that bear these chains.[6,7,9,10] For example, polyubiquitin chains linked via Lys48 of internal ubiquitin groups are used for signaling protein degradation, whereas Lys63-linked polyubiquitin chains, having different architecture, are used for receptor internalization, DNA repair, and protein−protein interactions in the nf-κB pathway. Functions of polyubiquitin chains of other linkage types are beginning to be assigned, some of which could also play an important role in cell cycle control (Lys11-linked polyubiquitin chains) and other signaling events, such as the linear Met1-linked chains in the nf-κB pathway.[11,12]

Most ubiquitination events are dynamically controlled by the action of deubiquitinating enzymes or DUBs (deubiquitinases), which counteract ubiquitination by hydrolytically removing ubiquitin from protein adducts. Deubiquitination is achieved by hydrolyzing the isopeptide bond after Gly76 (or the peptide bond in the case of Met1-linked polyubiquitin chains).[13−16] The human genome encodes for nearly 100 DUBS, which are emerging as key players in a wide array of physiological processes. Accordingly, deregulation of DUB activity has been linked to a number of human diseases such as cancer and neurodegeneration.[17−20] DUBs are grouped into five categories based on the structure of their catalytic domains: ubiquitin carboxy-terminal hydrolases (UCHs), ubiquitin specific proteases (USPs), Machado Joseph Disease proteases (MJDs), ovarian tumor proteases (OTUs) and JAB1/MPN/MOV34 proteases (JAMMs).[16,21] The first four groups are cysteine proteases, whereas the JAMM members are zinc metalloproteases, containing a catalytic zinc and sharing mechanistic similarities with the well-known zinc protease thermolysin.[21−23] Members of the zinc metalloprotease family include Rpn11 (POH1), a highly conserved proteasome component whose DUB activity is coupled to protein degradation at the proteasome, CSN5, the catalytic unit of the CSN deneddylating complex that regulates ubiquitination through cullin modification, AMSH, associated molecule with the SH3 domain of signal transducing adaptor molecule (STAM) and its yeast ortholog, Sst2, AMSH-LP (AMSH-like protein) with unknown function, and BRCC36 of the BRISC DNA repair complex.[24−31]

AMSH and AMSH-LP are highly selective for Lys63-linked polyubiquitin chains, the type of chain used in endosomal-lysosomal sorting of cell-surface receptors.[32−34] A key biological function of AMSH is to regulate degradation of cell-surface receptors in the lysosomes mediated by the ESCRT machinery, which comprises four distinct macromolecular complexes, ESCRT-0, ESCRT-I, ESCRT-II, and ESCRT-III.[35−37] The members of ESCRT machinery work in tandem to capture polyubiquitinated receptors on endosomes and sequester them into multivesicular bodies that eventually fuse with lysosomes where the receptors are degraded.[33,37−39] AMSH possesses binding sites for both the initial ESCRT-0 complex as well as the terminal ESCRT-III complex and plays an important role in regulating the ESCRT-mediated sorting process.[34,40,41] The catalytic activity of AMSH is enhanced upon binding to the STAM component of the ESCRT-0 complex.[42−44] The precise manner in which AMSH controls receptor trafficking through the ESCRT pathway remains unknown; however, its critical role in endosomal-lysosomal sorting is underscored by the recent discovery of a genetic defect known as microcephaly capillary malformation (MIC-CAP) syndrome, which is caused by mutations in the gene.[45,46]

The structural basis for high selectivity toward Lys63-linked polyubiquitin chains has been provided by the X-ray structural studies of AMSH-LP bound to Lys63-linked diubiquitin.[32] These structural studies, combined with the recent structure determination of Sst2 with Lys63-linked diubiquitin and ubiquitin (a part of the product), have revealed structural features in the active-site that contribute to substrate recognition and catalysis.[47] One such structural feature is a loop segment adjacent to the active-site cleft, referred to here as the active-site flap, that seems to open and close during catalytic steps of the enzyme (Figure 1a,b). The flap under consideration

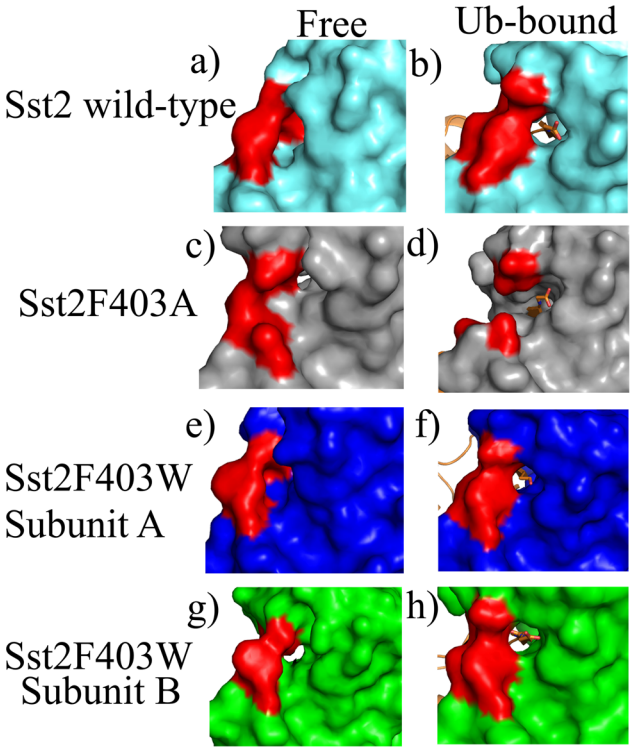

Figure 1. Changes in the active-site flap forming a closed cavity or a narrow tunnel in the cavity indicating the flexibility of the flap. (a), (c), (e), (g) Surface representations of active-site area of wild-type Sst2 (PDB ID: 4JXE) and its mutants in their free form. Residues that constitute either side of the flap (Asp315, Thr316, Leu402, and Phe403) are marked red. (b), (d), (f), (h) Surface representations of Sst2 (PBD ID: 4K1R) and its mutants bound to ubiquitin comparing the opening of the flap (red) in all structures. Wild-type Sst2 is shown in cyan, $Sst2^{F403A}$ in gray, $Sst2^{F403W}$ subunit A in dark blue and $Sst2^{F403W}$ subunit B in green. The Gly76 carboxylate group of ubiquitin is shown in sticks.

is part of a loop segment located in a structural element called insertion 2, a characteristic feature shared by AMSH and closely related enzymes, such as AMSH-LP and Sst2.[31] The flap in Sst2 is defined to encompass the tripeptide segment Gly401-Leu402-Phe403. The corresponding residues, Gly406-Phe407 in AMSH-LP and Gly394-Phe395 in AMSH, occur as a dipeptide segment as opposed to the tripeptide segment in Sst2 (Figure 2a−c). In the structure of the unbound enzyme, the flap is in a closed state, with a Phe residue in the flap making contact with residues on the opposite side of the cleft,

DOI: 10.1021/acs.biochem.5b00631
Biochemistry 2015, 54, 6038−6051

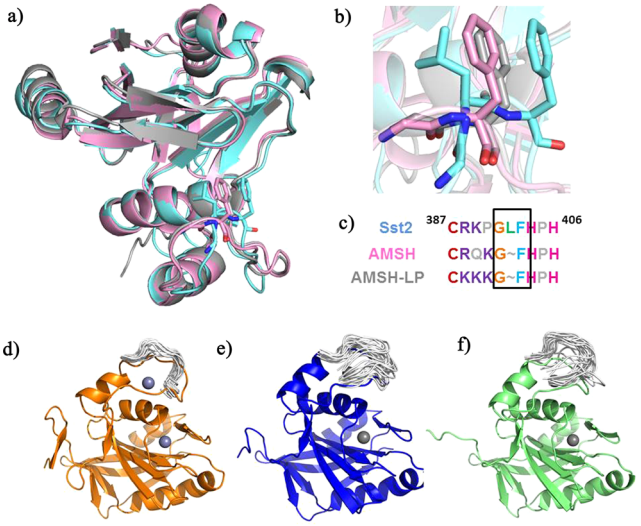

Figure 2. Structures of Sst2, AMSH, and AMSH-LP. (a) Superposition of the catalytic domain of Sst2 (PBD ID: 4JXE), AMSH (PDB ID: 3RZU), and AMSH-LP (PDB ID: 2ZNR). Sst2, AMSH, and AMSH-LP are shown in cyan, pink, and gray, respectively. (b) Stick representation of flap segment in Sst2, AMSH, and AMSH-LP. Sst2 consists of tripeptide segment in the flap, whereas AMSH and AMSH-LP consists of dipeptide segment. Sst2, AMSH, and AMSH-LP are shown in cyan, pink, and gray respectively (c) Sequence alignment of flap residues in Sst2, AMSH, and AMSH-LP. The inset represents the flap segment. (d–f) Conformational dynamics of the active site flap in Sst2, AMSH, and AMSH-LP: 20 equal-spaced snapshots were extracted from the molecular dynamics simulation and loop ensembles were superposed with their respective starting structures. The native protein conformation for Sst2, AMSH, and AMSH-LP are shown in orange, blue, and green cartoon representation respectively, with Zn^{2+} ions as gray spheres. All three enzymes Sst2 (d), AMSH (e), and AMSH-LP (f) are highly flexible in the flap region and sample conformations resembling open and closed states.

particularly with an Asp side chain (Asp 315 in Sst2), both of which are highly conserved in AMSH (yeast to human) and also in AMSH-LP. The distance between the aromatic ring and the carboxylate group is close to 4.0 Å, a feature shared with AMSH and AMSH-LP (Figure 3c). In the substrate-bound

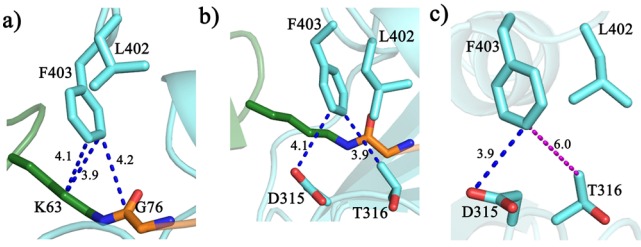

Figure 3. Phe403 forms interactions with the isopeptide linkage of the diubiquitin substrate and residues across the active-site cleft. (a) The scissile isopeptide is stabilized by several contacts with the aromatic group of Phe403 through interactions with both Lys63 of the proximal ubiquitin (forest green) and Gly76 of the distal ubiquitin (orange). (b) Upon binding of Lys63-linked diubiquitin (PDB entry 4NQL), Phe403 is stabilized by a 3.9 Å van der Waals contact between Phe403 and Thr316 and forms a 4.1 Å anion-π interaction between the ring of Phe403 and the carboxylate of Asp315. (c) Phe403 in its free form lost contact with Thr316 (6 Å shown in magenta) but forms 3.9 Å anion-π interaction between C_ζ of F403 and the carboxylate of Asp315. Hydrophobic interactions are shown in blue dashes.

state, Phe349 and Phe403 interacts with the aliphatic portion of the side chain of Lys63 of the proximal ubiquitin (in a diubiquitin motif, the Gly76 carboxylate group of one ubiquitin, called the distal ubiquitin, is covalently attached to the ε-amino group of a Lys residue of the other ubiquitin, called the proximal ubiquitin), whereas Thr347 and Ser352 form hydrogen bonds with Gln62 and Glu64, neighboring residues of Lys63, respectively. Indeed, the observation that Phe403 alone makes three van der Waals contacts with the isopeptide segment of diubiquitin seems to underscore its importance toward proper alignment of the isopeptide segment for catalysis (Figure 3a). It also appears that the Phe side chain, through its interaction with the facing Asp residue across the active-site cleft, may contribute to the dynamics of the flap, in addition to contributing key interactions with the Lys63 side group on the proximal ubiquitin (Figure 3b). To gain insight into the nature of the contribution of this flap residue to catalysis, we generated mutants of this conserved side chain by replacing with Ala, and with a bulkier aromatic side chain of Trp. These mutants were studied by a combination of X-ray crystallography of both free and ubiquitin-bound forms, enzyme kinetics, isothermal titration calorimetry (ITC), and molecular dynamics simulations.

MATERIALS AND METHODS

Cloning, Expression, and Purification. The catalytic domain of Sst2 (residues 245–435) and human ubiquitin (Ub) were subcloned into a pGEX-6P1 vector as described previously.[47] Phe403Ala, Phe403Trp, Asp315Asn, and Cys397Ala mutations were then introduced individually into the catalytic domain of Sst2 via site directed mutagenesis and confirmed with DNA sequencing. The resulting N-terminally fused glutathione-*S*-transferase (GST)-tagged recombinant DNA were expressed in *Escherichia coli* Rosetta cells and purified as described earlier[47] using standard GST affinity chromatography followed by size exclusion chromatography on a Superdex S75 column (GE Lifesciences). All proteins were concentrated, flash frozen, and stored at −80 °C. Final concentrations were determined via UV–vis by measuring absorbance at 280 nm.

In order to avoid issues arising from the cloning artifact in GST fusion proteins, addition of the pentapeptide sequence Gly-Pro-Leu-Gly-Ser (GPLGS) to the protein's N-terminus, ubiquitin used for ITC was instead prepared from a pRSETA plasmid as described earlier.[47] Lys63-linked diubiquitin was enzymatically synthesized using Lys63Arg and Asp77 ubiquitin mutants, following published methods.[32] Human E1, two E2s (Uev1a, and Ubc13), and the two mouse ubiquitin mutants were purified separately, then mixed in a reaction buffer containing 80 mM Tris-HCl, 20 mM ATP, 20 mM $MgCl_2$, 1 mM DTT. The reaction mixture was then incubated overnight at 37 °C, and quenched at room temperature with 10-fold excess Buffer A (50 mM sodium acetate pH 4.5). The quenched reaction mixture was loaded onto a MonoS cation exchange column (GE Healthcare) to separate synthesized diubiquitin from unreacted ubiquitin. Diubiquitin was eluted using a linear gradient with Buffer B (50 mM sodium acetate pH 4.5, 1 M NaCl).

Crystallization and Data Collection. Purified Sst2 Phe403Ala, Phe403Trp and ubiquitin were concentrated to 37, 6.7, and 40 mg/mL respectively. All crystallization was performed at room temperature by sitting drop vapor diffusion. Crystals of Sst2 Phe403Ala, referred to here as $Sst2^{F403A}$, were

DOI: 10.1021/acs.biochem.5b00631
Biochemistry 2015, 54, 6038–6051

crystallized in 0.8:1 ratio with the mother liquor containing 0.2 M sodium citrate tribasic dihydrate, 20% (w/v) polyethylene glycol (PEG) 3350 (pH 8.3) and were grown in 3−5 days. Crystals of Phe403Trp, referred to here as $Sst2^{F403W}$, were crystallized in 1:1 ratio with the mother liquor containing 0.2 M ammonium tartrate dibasic (pH 7.0) and 20% (w/v) PEG 3350 which attained maximum size in 5−7 days.

Noncovalent complexes of each Sst2 mutant and ubiquitin were prepared by mixing each mutant with ubiquitin (containing a N-terminal cloning artifact GPLGS, as a remnant of GST-affinity purification) at a ratio of 1.5:1. Crystals of the complex formed between $Sst2^{F403A}$ and Ub grew in a week from the mother liquor containing 0.2 M sodium citrate tribasic dihydrate, 0.1 M HEPES sodium pH 7.5, 20% v/v 2-propanol. Crystals of the complex of $Sst2^{F403W}$ and Ub were grown in 2−5 days in 0.04 M citric acid, 0.06 M Bis-TRIS propane pH 6.4, 20% w/v PEG 3350. Complex formation of both constructs was verified by silver staining of an SDS-PAGE gel run with dissolved crystals.

Crystals were soaked briefly in a cryoprotectant solution of 25% (v/v) ethylene glycol in the mother liquor and flash frozen with liquid nitrogen. X-ray diffraction data for all described mutants and protein complexes were collected at 100 K using a Mar300 CCD detector at beamline 23 ID-B of the Advanced Photon Source at Argonne National Laboratory in Argonne, IL and processed with HKL2000 program.[48]

Structure Determination and Refinement of $Sst2^{F403A}$ and $Sst2^{F403W}$ in Its Free Form. The structures of $Sst2^{F403A}$ and $Sst2^{F403W}$ mutants, which crystallized in the $P2_1$ space group and diffracted to 2.1 and 1.6 Å, respectively, were solved by molecular replacement with MolRep[49] of the ccp4 suite[50] using the previously solved structure of the catalytic domain of Sst2 (PDB entry 4JXE) as the search model.[47] Initial refinements for each structure were carried out in Refmac5 using rigid body refinement followed by restrained refinement. The model for $Sst2^{F403A}$ was built using Coot[51] and refined using the program Refmac5[52] yielding R_{crys} and R_{free} values of 20.04% and 24.18% respectively. The model for $Sst2^{F403W}$ was built in Coot and rounds of refinement of refinement were done in PHENIX,[53] ultimately yielding a R_{crys} of 17.0% and R_{free} of 19.9%.

Structure Determination and Refinement of $Sst2^{F403A}$-Ub and $Sst2^{F403W}$-Ub structures. Crystals of $Sst2^{F403A}$ bound to ubiquitin, referred to here as $Sst2^{F403A}$-Ub, crystallized in the $P2_1$ space group and diffracted to 1.7 Å, while the crystal structure obtained for $Sst2^{F403W}$ bound to ubiquitin, referred to here as $Sst2^{F403W}$-Ub, belonged to the $P2_12_12_1$ space group and diffracted to 2.3 Å. Both structures were solved by molecular replacement using MolRep[49] using the previously solved structure of the catalytic domain of Sst2 bound to ubiquitin (PDB entry 4K1R) as the search model. Initial refinements were carried out in Refmac5[52] using rigid body refinement followed by restrained refinement. The model for $Sst2^{F403A}$-Ub was built using Coot[51] and refined using Refmac5[52] yielding R_{crys} and R_{free} values of 20.07% and 23.81%, respectively. During refinement, TLS treatment of atomic displacement parameters was also performed, taking chain A of the asymmetric unit as one group.[54] Likewise, a model for $Sst2^{F403W}$-Ub was built using Coot, and rounds of refinement of refinement were done in PHENIX,[53] ultimately yielding a R_{crys} of 19.2% and R_{free} of 23.5%. All figures for the structures described were rendered with PYMOL (version 1.7.0.0).[55]

Determination of Kinetic Parameters. Kinetic parameters of diubiquitin cleavage by $Sst2^{F403A}$ and $Sst2^{F403W}$ mutants were determined by incubating 100 nM of the enzyme with varying concentrations of Lys63-linked diubiquitin, ranging from 20 to 100 μM in a reaction mixture consisting of 50 mM Tris-HCl (pH 7.0), 20 mM KCl, 5 mM $MgCl_2$, and 1 mM DTT. For $Sst2^{C397A}$, 2 μM of the enzyme was used for diubiquitin cleavge. Reactions proceeded at room temperature for 15 min before quenching with 5× SDS-PAGE sample buffer. Samples were loaded and run on an SDS-PAGE gel along with 6, 20, and 40 μM ubiquitin standards. Ubiquitin bands were quantified and integrated using ImageJ[56] and plotted with a calibration plot of the previously mentioned standards in order to determine the amount of ubiquitin produced through the cleavage of diubiquitin. All data was analyzed with Kaleidagraph and fit to the Michaelis−Menten equation of $V_i = (V_{max}[S])/(K_M + [S])$ to determine k_{cat} and K_M for each mutant.

Circular Dichroism. The secondary structure of wild-type Sst2, the active-site flap mutants $Sst2^{F403A}$ and $Sst2^{F403W}$ and the $Sst2^{C397A}$ mutant was determined in solution using circular dichroism (CD). Protein samples were diluted in 100 mM phosphate buffer (pH 7.4) to make a final concentration of 0.2 mg/mL. Native CD spectra were recorded in a Jasco J-1500 spectrophotometer in the far-UV region (200−260 nm) in a cuvette with a path length of 0.1 cm. To test the stability of the mutants in solution, we also monitored changes in ellipticity at 222 nm via thermal melt by heating the protein from 20 to 86 °C with a temperature gradient of 0.5 °C. Data were recorded after every increase of 2 °C. Each spectrum was composed of an average of four scans (speed scan of 100 nm/min) and corrected with a subtraction of a spectrum of the phosphate buffer alone. Mean residue molar ellipticity was calculated according to the following equation:

$$[\theta] = (\theta \times 100M)/(Cln)$$

where θ is the ellipticity in degrees, l is the path length in centimeters, C is the concentration is mg/mL, M is molecular mass, and n is the total number of residues in the protein. Calculated mean residue molar ellipticity is given in deg cm^2 $dmol^{-1}$. The protein secondary structures from CD spectra were estimated using two different analysis tools: K2D2[57] and K2D3.[58]

ITC. ITC experiments were carried out at 25 °C in order to quantify the binding affinity of the Sst2 mutants with ubiquitin using a GE/MicroCal ITC_{200} calorimeter. The proteins were dialyzed overnight in a buffer of 50 mM Tris-HCl (pH 7.6) and 50 mM NaCl that was exchanged four times. 500 μM ubiquitin was titrated into a 50 μM solution of protein. Twenty-two injections with 1.4 μL of ubiquitin per injection were done for the experiment. 180 s was allowed between each injection to ensure that baseline was reached prior to the next injection. Baseline correction was performed by NITPIC[59] and analyzed using a one-site model from SEDPHAT.[60]

Diubiquitin Cleavage Assay. A diubiquitin cleavage assay was performed in order to deduce whether the mutants were able to cleave Lys11-linked and Lys48-linked diubiquitin chains in addition to Lys63-linked diubiquitin. 250 nM of wild-type and mutant enzymes were incubated in a reaction of 50 mM Tris-HCl (pH 7.0), 20 mM KCl, 5 mM $MgCl_2$, and 1 mM DTT in the presence of 20 μM of each variant of diubiquitin. Reactions were allowed to occur at room temperature for 5 h before being quenched with 5× SDS-PAGE sample buffer.

DOI: 10.1021/acs.biochem.5b00631
Biochemistry 2015, 54, 6038−6051

Samples were loaded and run on an SDS-PAGE gel and ubiquitin bands were quantified and integrated using ImageJ.[56] Ratios of monoubiquitin:diubiquitin were determined for each sample after the reactions.

Molecular Dynamics Simulations. We performed molecular dynamics simulations within the Amber14 package[61] to investigate molecular motions in three apo Sst2 systems: native enzyme, $Sst2^{F403A}$, and $Sst2^{F403W}$ mutants. Therefore, we used the previously reported crystal structure of the native enzyme (PDB: 4JXE)[47] as well as the newly reported structures of the $Sst2^{F403A}$ and $Sst2^{F403W}$ mutants as starting configurations. Additionally, we investigated the homologous enzymes AMSH and AMSH-LP using starting coordinates from published crystal structures (PDB: 3RZU[40] and PDB: 2ZNR).[32] We discarded ethylene glycol and other cocrystallized small molecules and prepared all proteins using MOE's protonate3D function for simulations.[62] The five systems were parametrized using the Amber force field 99SB-ILDN[63] and soaked in an explicit box with TIP3P water molecules[64] with a minimum wall distance of 10 Å. Two Zn^{2+} ions were included per system using nonbonded parameters suggested by the R.E.D. server[65] (r = 1.95 Å, e = 0.25 kcal/(mol·cm)) and were held in place over simulation time by applying flat bottom harmonic restraints to the coordinating amino acids.

After a careful equilibration[66] we sampled conformational space over 1 μs and saved 50 000 snapshots per system for later analysis. Simulation analysis was performed using cpptraj from Ambertools[67] as well as in-house scripts. We quantified global dynamics of the Cα of the conserved Phe residue (F403 in Sst2, F395 in AMSH, and F407 in AMSH-LP) as B-factor after performing a global alignment to all Cα atoms in the enzymes. Furthermore, we characterized local dynamics of the backbone atoms of this residue by following a local alignment strategy.[68] Additionally, we estimated dihedral entropies for all backbone torsions involving the conserved residue.[69] Hydrogen bonds were extracted using cpptraj's default criteria.

RESULTS

Design of the Mutants. The crystal structure of the catalytic domain of AMSH-LP bound to its substrate Lys63-linked diubiquitin (PBD ID: 2ZNV) reveals the flap adopting a closed position over the active site.[32] Specifically, the flap appears to have collapsed around the isopeptide bond, particularly onto the aliphatic portion of the side chain of Lys63 from the proximal ubiquitin, bringing Phe407 (Phe403 in Sst2) into close van der Waals contact with the side chain atoms of the Lys residue. The recently determined crystal structure of the catalytic domain of the yeast AMSH ortholog, Sst2, bound to Lys63-linked diubiquitin reiterates this observation (Figure 3a).[47] The proximity of the aromatic side group of the Phe residue to the Lys63 side chain moiety of the scissile isopeptide bond is indicative of a role in substrate recognition and/or catalysis. In addition to the scissile isopeptide bond, Phe403 is stabilized by a 3.9 Å van der Waals contact between Cζ of Phe403 and Cγ of Thr316 and a close contact (4.1 Å) between Cδ1 of the Phe403 ring and Oδ of the carboxylate of Asp315 (Figure 3b). Interestingly, a recent analysis of such distance pairs in the Protein Data Bank has revealed some evidence of an anion-π interaction, a stabilizing interaction between the partially electropositive edge of the aromatic ring with the negatively charged Asp (or Glu) residue that is proposed to contribute toward protein stabilization and protein−protein interactions.[70] The active-site flap also assumes a slightly different closed conformation in structures of the substrate-free form of the enzyme (AMSH, AMSH-LP, and Sst2). In Sst2, the van der Waals contact with Thr316 has been lost due to repositioning of the aromatic group from Phe403 such that the Cζ of Phe403 now forms a 3.9 Å anion-π interaction with Oδ of the carboxylate of Asp315 (Figure 3c).

Although the flaps form a narrow tunnel near the active site cavity in the enzyme's closed state, as seen in structures of both the free and substrate-bound forms of Sst2, PBD ID: 4JXE and 4NQL, respectively, the flaps must open for the substrate to bind in a proper orientation so that the C-terminal tail of the distal ubiquitin, particularly the scissile isopeptide bond, is adjacent to the catalytic center. Thus, the flap must be intrinsically dynamic, oscillating between an open and closed form so that the enzyme can bind its substrate in the open form and interact with the Lys63 side chain of the proximal ubiquitin in the closed from. The crystallographic B-factors of residues in the flap are consistent with the dynamic nature of the flap (Supplemental Table 1). To explore this further, microsecond molecular dynamics simulations of Sst2, AMSH, and AMSH-LP were carried out, which confirmed that the active-site flap is indeed quite mobile in all these proteins (Figure 2d−f). During the time scale of the simulation, the conserved Phe residue explored both multiple side chain conformations and increased mobility of the backbone atoms (this is discussed further below). On the basis of the results from the MD simulation, along with the crystallographic observations of substrate-bound and free enzymes (AMSH-LP and Sst2), we decided to focus on the conserved Phe residue to probe the possible role of the dynamics of the flap in catalysis. In the closed, substrate-bound form, the van der Waals interactions between the aromatic ring of Phe403 and the Lys63 side chain of the proximal ubiquitin appear to be important for the rate-limiting step rather than ground-state substrate binding, based on the following observations. First, mutation of this residue to Ala in both AMSH-LP and AMSH causes a significant loss only in k_{cat} with relatively minor change in K_M.[32,44] Second, ITC data show that the affinity for diubiquitin is similar to that for ubiquitin alone (bound in the distal site), implying that interactions with the entire proximal ubiquitin portion of the substrate contributes little to ground-state substrate affinity.[44,47]

It is possible that mutation of the Phe residue to Ala might have caused a change in dynamic properties of the flap accounting for the loss of activity, at least to some degree. In other words, the conserved Phe side chain may have a role in modulating the dynamics of the flap to be in tune with the catalytic steps of the hydrolysis reaction. To gain insight into the nature of the catalytic contribution of Phe403 in polyubiquitin processing, and hence the role played by the active-site flap, we mutated Phe403 in Sst2 to Trp and Ala. We expected that the presence of a bulkier aromatic side chain in the Trp mutant may alter the dynamic properties of the flap by providing a larger surface area for contact with the residues opposite the active-site cleft (such as the γ-CH3 group of Thr316, Figure 3) while still maintaining the contacts necessary for accurate positioning of the isopeptide segment of Lys63-linked polyubiquitin chains. Although the mutation of the corresponding Phe to Ala residue was recently studied in both AMSH-LP and AMSH for its role in catalysis,[32,44] these previous studies lacked structural and binding characterization of the Ala mutant, so one could not rule out other factors such as change in ubiquitin binding affinity (product release) or

DOI: 10.1021/acs.biochem.5b00631
Biochemistry 2015, 54, 6038−6051

structural changes arising from the mutation accounting for the loss of activity in the mutant.

Kinetic Characterization of the Flap Mutants. Mutation of Phe403 to Ala leads to a substantial loss of catalytic activity, with a major effect on k_{cat} while K_M remains relatively unchanged compared to the wild-type enzyme (Table 1, Figure 4, and Supplemental Figure 2), consistent with observations from the same mutant in AMSH-LP and AMSH.[32,44] This suggests that the role of the aromatic side chain is conserved from the yeast enzyme to human counterparts. Like the Ala mutant, the Phe403Trp mutant exhibits a significant defect in catalyzing the deubiquitination reaction, with a reduction mainly in k_{cat} and a minimal effect on K_M (Table 1, Figure 4, and Supplemental Figure 2). Taken together, these kinetic results implicate a role for Phe403 mainly in the rate-limiting step, since both of these mutations led to a loss in k_{cat} and not in ground state substrate binding indicated by a relatively minor change in K_M.

As mentioned before, the flap constitutes the tip of a structural element in AMSH-like enzymes known as insertion 2 (Supplemental Figure 1). The insertion 2 region is stabilized by the presence of a structural zinc atom, coordinated by a three histidine, 1 cysteine motif that provides rigidity to the overall structure. Since the tip of the flap is arranged distally from the zinc-coordination site, it is flexible enough to allow for oscillation between open and closed conformations during key catalytic steps of the enzyme. The absence of the structural zinc would render insertion 2 highly disordered. Accordingly, mutation of a zinc-coordinating residue, Cys397, to Ala leads to a substantial loss of activity, once again with a reduction only in k_{cat} (Table 1, Figure 4, and Supplemental Figure 2). This is consistent with the results obtained with a similar mutant in AMSH-LP (Cys402 to Ser).[32] It is possible that the insertion, having lost its native structure due to impaired binding of the structural zinc atom, might have adopted a non-native fold keeping the flap away from the active-site cleft, which would make the Phe residue less accessible for binding to the isopeptide moiety of the substrate during catalysis. Alternatively, the extreme conformational flexibility may mean a higher entropic penalty in organizing the flap into a productive orientation during the rate-determining step of the hydrolysis reaction.

Structural Properties of the Flap Mutants. We wondered whether mutation of Phe403 to Ala or Trp reduced the enzyme's catalytic efficiency by imposing either global changes to the protein's overall structure or by imparting structural changes in the local environment of the active site flap that manifest as either altered dynamics or impaired ability to recognize and bind the substrate. To address the effect of each mutation, we crystallized both the Sst2^{F403A} and the Sst2^{F403W} mutants in their apo and ubiquitin-bound forms. Diffraction data collection and refinement statistics are summarized in Table 2. The structures were solved by molecular replacement using the previously solved wild-type structure of Sst2 (PDB ID: 4JXE) as the search model for both apo structures and the previously solved structure of Sst2 bound to ubiquitin (PDB ID: 4K1R) as the search model for both ubiquitin-bound mutant structures. Crystals of Sst2^{F403A} (apo) and Sst2^{F403A}-Ub diffracted to 2.1 and 1.7 Å, respectively, while Sst2^{F403W} (apo) and Sst2^{F403W}-Ub diffracted to 1.6 and 2.3 Å, respectively. The free R factors after refinement for all structures were within 2.5−4.3% of crystallographic R factors.

Table 1. Steady-State Kinetic Parameters of Sst2 and Its Substrate, Lysine 63-Linked Diubiquitin

sample	K_M (μM)	k_{cat} (s^{-1})	$k_{cat}/K_M \times 10^{-3}$ (μM^{-1} s^{-1})
Sst2	18.8 ± 8.4	1.5 ± 0.2	79.8
Sst2^{F403A}	33.6 ± 8.3	0.082 ± 0.007	2.4
Sst2^{F403W}	44.1 ± 8.2	0.085 ± 0.007	1.9
Sst2^{C397A}	32.8 ± 4.6	0.004 ± 0.0002	0.1
Sst2^{D315N}	33.7 ± 11.8	0.26 ± 0.032	7.7

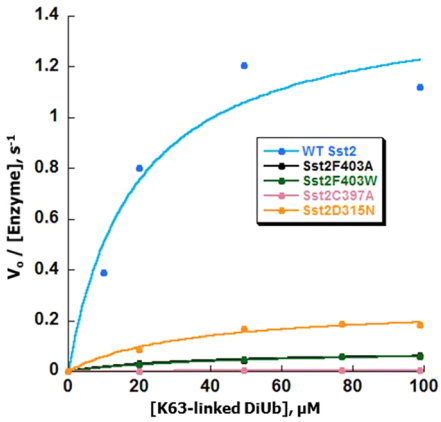

Figure 4. Activity of active-site flap mutants compared to wild-type Sst2.

The structure of the Sst2^{F403A} mutant in its free form shows that, as in the wild-type enzyme, the flap assumes a closed form. A minor difference is that a narrow tunnel has formed in the cavity due to the absence of the aromatic side chain, which can no longer form the anion-π interaction with Asp315 from the adjacent loop (Figure 1c). Ubiquitin binding to Sst2^{F403A} leads to formation of a wider cavity with a more open conformation, instead of a narrow tunnel observed in the wild-type, Sst2-Ub structure (Figure 1d). Despite the more open conformation of the Sst2^{F403A} mutant, the C-terminal tail of ubiquitin maintains the same orientation observed in the ubiquitin-bound structure of wild-type Sst2. The Ala residue appears to be somewhat more disordered as judged from the weak electron density enveloping the side chain as compared to internal residues that are defined by stronger electron density covering the side chain, consistent with an increased flexibility of the flap in the mutant (Supplemental Figure 3c,d and Supplemental Table 1). However, the structures of both the free and ubiquitin-bound forms indicate that the mutation to Ala does not have any serious effect on either the overall structure or the active-site area of the enzyme. Moreover, circular dichroism (CD) spectroscopy indicated no major perturbation in secondary structure for either Sst2^{F403A} or Sst2^{F403W} in solution (Figure 5a, Supplemental Table 2). Deconvolution of the CD spectra of mutants produced similar α-helical and β-sheet content as in the wild-type protein (Supplemental Table 2). Thermal melting performed using CD also revealed nearly identical melting temperatures for the Sst2^{F403A} mutant and the wild-type enzyme, indicating the overall stability of the enzyme is unaffected by mutation of Phe403 to Ala (Figure 5b, Table 3). Interestingly, reduced affinity for the structural zinc metal, and thus increased disorder of the insertion 2 segment, led to a drastic reduction in melting temperature for the Sst2^{C397A} mutant (Figure 5 and Table 3).

DOI: 10.1021/acs.biochem.5b00631
Biochemistry 2015, 54, 6038−6051

Table 2. Crystallographic Refinement Statistics for Catalytic Domain of Sst2

	Sst2 F403A	Sst2 F403A-Ub	Sst2 F403W	Sst2 F403W-Ub
Data collection				
space group	$P2_1$	$P2_1$	$P2_1$	$P2_12_12_1$
cell dimensions				
a, *b*, *c* (Å)	57.7, 74.9, 64.6	42.1, 58.2, 56.4	58.6, 73.7, 64.6	56.8, 89.4, 117.8
α, β, γ (deg)	90.0, 112.9, 90.0	90.0, 109.3, 90.0	90.0, 113.2, 90.0	90.0, 90.0, 90.0
wavelength (Å)	1.033	1.033	1.033	1.033
resolution (Å)	50.0−2.1 (2.14−2.10)	50.0−1.7 (1.75−1.72)	50.0−1.6 (1.66−1.63)	50.0−2.3 (2.34−2.30)
R_{merge} [b] (%)	10.5 (73.3)	4.7 (56.1)	9.5 (56.2)	13.1 (84.8)
$I/\sigma I$	11.6 (2.0)	23.6 (2.3)	18.1 (2.5)	18.7 (2.3)
completeness (%)	99.9 (99.9)	99.9 (99.9)	97.3 (96.2)	100.0 (100.0)
redundancy	3.8 (3.8)	3.8 (3.6)	3.9 (7.7)	14.6 (13.8)
Refinement				
resolution (Å)	2.1	1.7	1.6	2.3
no. unique reflections	28834	26060	60880	25792
R_{work} [c]/R_{free} [d]	20.0/24.2	20.1/23.7	17.0/19.9	19.2/23.5
no. atoms				
protein	2926	2027	2946	4059
ion	4	2	4	4
water	93	43	151	79
r.m.s. deviations				
bond lengths (Å)	0.018	0.018	0.007	0.015
bond angles (Å)	1.935	1.896	1.111	1.728
Ramachandran Plot				
preferred (%)	97.1	96.46	98.3	95.9
allowed (%)	2.9	3.2	1.7	3.7
disallowed (%)	0.0	0.39	0	0.39
average *B*-factors (Å^2)				
Sst2	32.5	18.9	24.4	42.8
ubiquitin		39.9		47.1
ion	28.0	34.2	20.0	40.8
water	31.0	38.0	30.0	41.1
ligand	42.6	33.4	43.5	51.6

[a]Values in parentheses are for the highest resolution shell. [b]$R_{merge} = \sum|I_{hkl} - I_{hkl(j)}|/\sum I_{hkl}$, where $I_{hkl(j)}$ is the observed intensity and I_{hkl} is the final average intensity. [c]$R_{crys} = \sum||F_{obs}| - |F_{calc}||/\sum|F_{obs}|$. [d]$R_{free} = \sum||F_{obs}| - |F_{calc}||/\sum|F_{obs}|$, where R_{free} and R_{crys} are calculated using a randomly selected test set of 5% of the data and all reflections excluding the 5% test data, respectively.

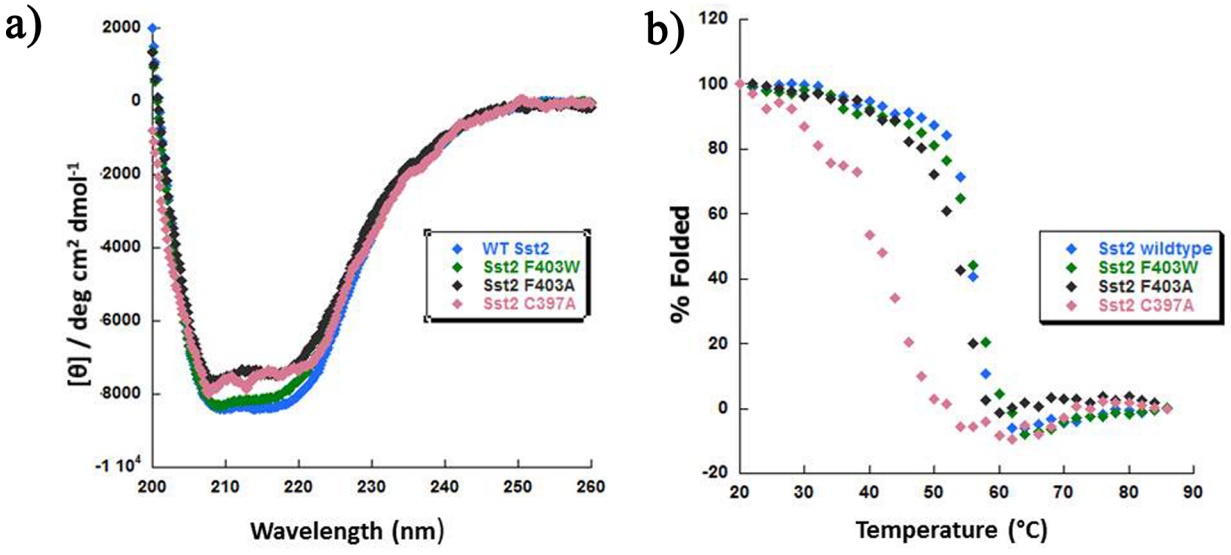

Figure 5. Circular dichroism (CD) spectroscopy of Sst2 and its mutants. (a) Native CD spectra of catalytic domain of Sst2, Sst2^{F403A}, and Sst2^{F403W} show that the secondary structure of the enzyme is mostly unperturbed in solution as a result of either mutation. (b) Thermal melting curves indicate nearly identical melting temperatures of the F403 mutants with wild-type Sst2, suggesting that the stability of the enzyme in its folded state is retained in the mutants. The thermal melting curve for the Sst2^{C397A} mutant indicates that this mutant is less stable than F403 mutants and wild-type Sst2.

DOI: 10.1021/acs.biochem.5b00631
Biochemistry 2015, 54, 6038−6051

Table 3. Stability Parameters Deduced from CD Data

sample	T_M (°C)	222/209 ratio
Sst2	56	0.87
$Sst2^{F403A}$	55	0.89
$Sst2^{F403W}$	56	0.91
$Sst2^{C397A}$	40	0.89

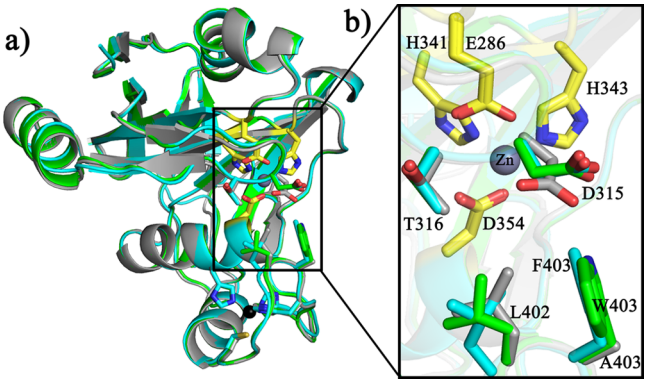

Figure 6. Structural comparison of Sst2 and its mutants. (a) Superposition of catalytic domain of Sst2 (cyan), $Sst2^{F403A}$ (gray), and $Sst2^{F403W}$ (green) indicate no gross conformational changes to Sst2 as a result of either mutation. (b) Superposition of Sst2 (cyan), $Sst2^{F403A}$ (gray), and $Sst2^{F403W}$ (green) highlighting the residues of active-site along with the residues of the active-site cleft. Active-site residues are colored in yellow. Active-site zinc is shown in gray whereas the zinc stabilizing insertion 2 is shown in black.

Figure 6 shows key areas near the active-site cleft in the mutant as compared to those in the wild-type enzyme. There is little difference between the structures in the environment around the active-site metal. The $Sst2^{F403A}$ structure also explains why the K_M of the mutant is similar to that of the wild-type enzyme; the contacts with the distal ubiquitin are maintained nearly identically with respect to the wild-type enzyme (Figure 7). To probe if these interactions are indeed maintained in solution, we performed isothermal titration calorimetry (ITC) studies to extract the binding affinity of the mutant for ubiquitin (Table 4, Figure 8a), which yields K_D values somewhat similar to that obtained with wild-type enzyme. Together, with the aforementioned results, our structural analysis provides strong support in favor of the assertion that the loss in activity of the Ala mutant is neither due to any gross structural change near active-site cleft induced by the mutation nor due to changes in substrate binding (K_M is not affected significantly). Furthermore, it seems unlikely that product release would be affected due to the mutation since the K_D for ubiquitin is comparable for the Ala mutant relative to the wild-type enzyme. For the Trp mutant, the K_D for ubiquitin binding is nearly 3 times lower than that of the wild-type enzyme which may indicate some level of interference in product release caused by the mutation; however, this cannot be a major factor behind the loss of activity in the mutant compared to the wild-type enzyme as the mutant is impaired nearly 30 fold in k_{cat}, whereas the change in product affinity is only by a factor of ~3.

The Trp mutant in both its free form and ubiquitin-bound form crystallizes with two subunits in the asymmetric unit. Both subunits in the free and ubiquitin-bound forms can be superimposed with each other with Cα root-mean-square deviations (RMSDs) of 0.198 and 0.304 Å, respectively,

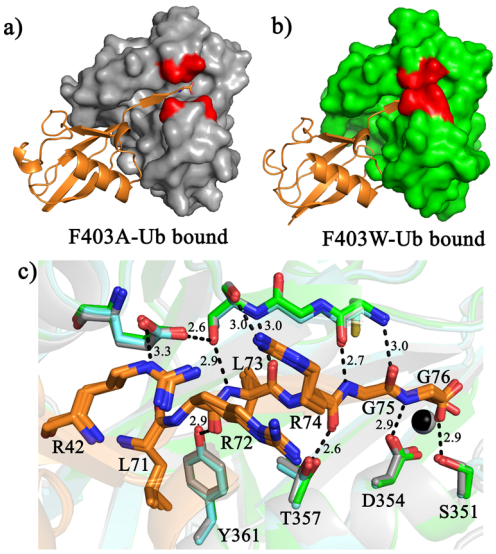

Figure 7. Ubiquitin binding in Sst2 mutants. (a) Surface representation of the catalytic domain of Sst2 mutant $Sst2^{F403A}$ (gray) bound to ubiquitin (orange). Residues of the flap region are highlighted in red. (b) Surface representation of the catalytic domain of mutant $Sst2^{F403W}$ (green) bound to ubiquitin (orange) highlighting the residues (red) in the flap region. (c) Superposition of the structures of Sst2 (cyan), $Sst2^{F403A}$ (gray), and $Sst2^{F403W}$ (green) showing residues involved in distal ubiquitin recognition. Hydrogen bonds are shown in black dashes. Ubiquitin residues are shown in orange.

Table 4. Thermodynamic Parameters Deduced from ITC Data

protein	titrant	K_D (μM)	ΔH (kcal/mol)	ΔS (cal mol^{-1} K^{-1})
Sst2	Ub	10.2 ± 0.6	11.9 ± 0.4	62.9
$Sst2^{F403A}$	Ub	6.2 ± 0.5	12.1 ± 0.4	64.3
$Sst2^{F403W}$	Ub	3.6 ± 0.3	12.8 ± 0.4	67.9
AMSH-LP	Ub	17.3 ± 4.3	1.95 ± 0.4	28.3
$AMSH\text{-}LP^{C402S}$	Ub	12.4 ± 3.2	8.5 ± 2.0	51.0

indicating structural conservation between the two subunits. Interestingly, both the subunits show a slight change around the flap region. Subunit A of the free form reveals a closed form of the flap with a completely occluded cavity resembling that of wild-type Sst2, whereas subunit B shows that the flap is also in a closed form, but has a narrow tunnel in the cavity (Figure 1e,g). The ubiquitin-bound structure reveals that in subunits A and B, the active site flap forms a narrow channel around the C-terminal tail of ubiquitin (or what would be the distal ubiquitin moiety in diubiquitin), which would be used to enable binding of the isopeptide linkage of diubiquitin. Strikingly, the size of the tunnel in subunit B appears to be wider than subunit A (Figure 1f,h). These subtle changes indicate that the dynamics of the flap in the Trp mutant are consistent with the lack of strong electron density enveloping the side chain of Trp, especially in subunit B of both the free form and the ubiquitin-bound form as shown in (Supplemental Figure 3b and Figure 9b). There is also a difference in the crystallographic contacts of the two subunits in both the free form and in the ubiquitin-bound form. In the free form, the Trp side chain of subunit A appears to be interacting with Thr345 of subunit B from its symmetry mates, whereas the Trp side chain of subunit B does not appear to form any interactions (Supplemental Figure 4a).

DOI: 10.1021/acs.biochem.5b00631
Biochemistry 2015, 54, 6038−6051

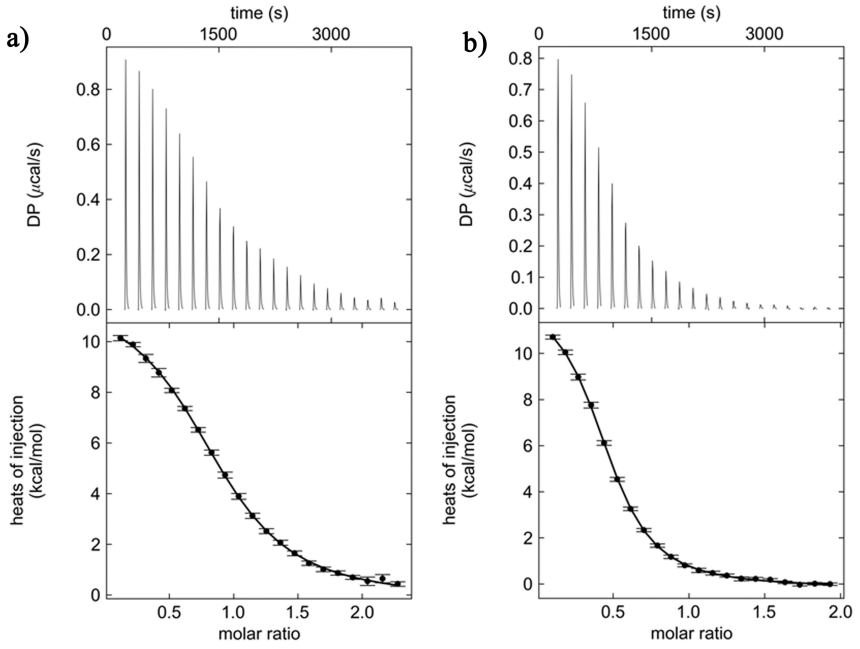

Figure 8. Determination of thermodynamic parameters for Sst2 mutants: (a) Isothermal titration calorimetry (ITC) thermogram for binding of ubiquitin to the catalytic domain of $Sst2^{F403A}$ revealing a K_D of 6.2 ± 0.5 μM. (b) ITC thermogram of binding of ubiquitin to the catalytic domain of $Sst2^{F403W}$ revealing a K_D of 3.6 ± 0.3 μM.

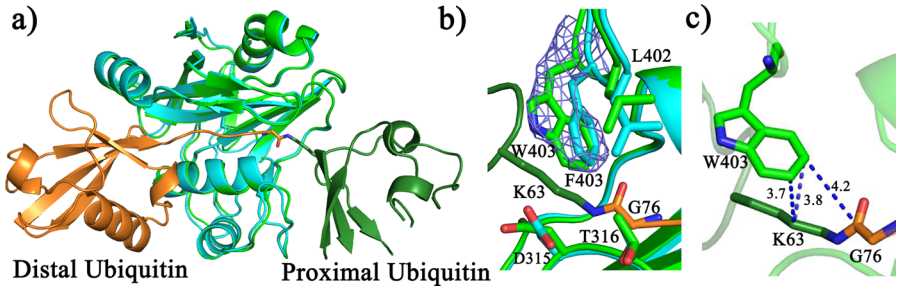

Figure 9. A model of $Sst2^{F403W}$ bound to Lys63-linked diubiquitin. (a) Superposition of catalytic domain of $Sst2^{F403W}$ (green) bound to ubiquitin and the catalytic domain of Sst2 (cyan) bound to Lys63-linked diubiquitin (PDB ID: 4NQL). The proximal ubiquitin and distal ubiquitin is shown in forest green and orange, respectively. (b) Superposition of $Sst2^{F403W}$ (green) bound to ubiquitin and Sst2 (cyan) bound to Lys63-linked diubiquitin showing the active-site flap residues. The electron density for Trp403 is rendered from the $2F_o$-F_c map contoured at 1σ (corresponding to the X-ray structure of $Sst2^{F403W}$ bound to ubiquitin) showing weak density enveloping the side chain of Trp403. (c) Hydrophobic interaction of the aromatic group of Trp403 interacts with Lys63 of the proximal ubiquitin (forest green) and Gly76 of the distal ubiquitin (orange). Hydrophobic interactions are shown in blue dashes.

Likewise, in the ubiquitin-bound form, the Trp side chain of subunit A appears to be held in place in the crystals by an additional interaction with the Lys48 side chain of the other ubiquitin-bound complex of the asymmetric unit (Supplemental Figure 4b). It is possible that the structural difference at the Trp residue between the two subunits may be a result of these crystallographic contacts. However, overall inspection of the structures reveals no appreciable change in the enzyme that could result from the mutation. Ubiquitin is bound in an identical fashion as in the wild-type enzyme and the Ala mutant (Figure 7).

Thermal melting using CD spectroscopy revealed a comparable melting temperature with respect to both the wild-type enzyme and the Ala mutant (Table 3 and Figure 5). Moreover, ITC studies also reveal similar affinity for ubiquitin and thermodynamic parameters to the wild-type enzyme (Table 4, Figure 8b). Collectively, our structural studies indicate that the loss of activity observed with the Trp mutant is not due to any gross structural changes from the mutation that may impair substrate and product binding.

Increased Dynamics of the Phe403Trp Active Site Flap. We expected that, unlike the Ala mutant, stabilizing interactions with the substrate (Lys63 side chain of the isopeptide link) in the Trp mutant would be maintained as in the wild-type enzyme. Using the crystal structure of the $Sst2^{F403W}$ bound to ubiquitin and the structure of Sst2 bound to diubiquitin (PDB ID: 4NQL), we generated a structural model of the mutant bound to Lys63-linked diubiquitin to gain insight into interactions with the substrate. The model shows that the side group of Trp is not in any steric conflict with any part of the proximal ubiquitin (consistent with the K_M of the mutant not changing appreciably compared to the wild-type enzyme). Remarkably, the side chain of Trp403 in the mutant overlaps nicely onto the side chain of Phe in the wild-type enzyme, indicating that the isopeptide interaction would be maintained during key catalytic steps of the hydrolysis reaction (Figure 9 shows a superposition of the mutant onto the crystal structure

DOI: 10.1021/acs.biochem.5b00631
Biochemistry 2015, 54, 6038−6051

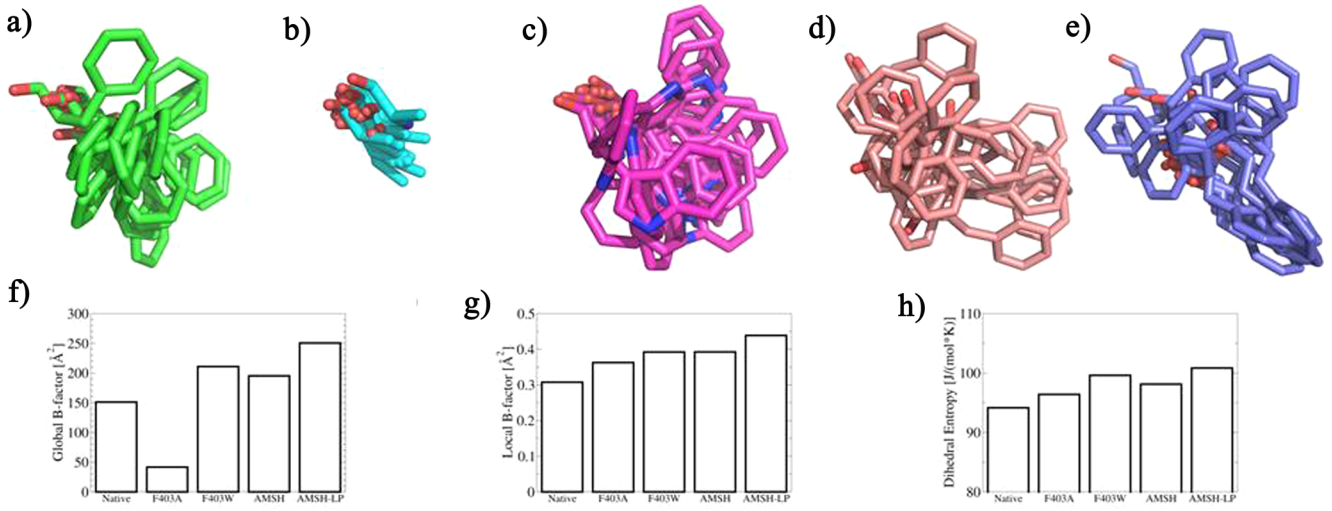

Figure 10. Molecular dynamics of the active site flap in native Sst2, the Phe403Ala and Phe403Trp mutants as well as AMSH and AMSH-LP: (a–e) Ensembles of 20 conformations extracted over 1 μs simulation time in equal spacing depict the high mobility of the respective side chains. Almost free rotation is observed for all residues, including the bulky aromatic systems in the native enzyme, the Phe403Trp mutant, AMSH and AMSH-LP. Phe403, Ala403, Trp403 in Sst2 are shown in green, blue and dark pink respectively, Phe395 in AMSH is shown in light pink and Phe407 in AMSH-LP is shown in purple. (f) B-factors of the Cα atom of the conserved phenylalanine and mutant residues after a global alignment, thus depicting loop flexibility. Aromatic residues show highest flexibility in the flap region. (g) An increase of intrinsic flexibility is observed for both mutants when capturing flexibility via B-factor calculation after a local alignment to the backbone atoms. (h) Dihedral entropies over backbone torsions involving residue 403 in Sst2 indicate a similar trend as the local backbone B-factors, thus confirming gains in loop flexibility by mutations at this position.

of the wild type Sst2 bound to diubiquitin). Thus, the loss in activity of the Trp mutant, as reflected by the reduction in k_{cat}, is not due to a lack of van der Waals interactions that facilitate catalysis of Lys63-linked diubiquitin.

It is plausible that the loss of activity is due to altered dynamics of the flexible flap in the Trp mutant although one expects a similar anion-π interaction with Asp315 involving the six-membered ring of the Trp side chain. We probed this effect by performing molecular dynamics simulations of the native system and the two mutants on the microsecond time scale and compared flap dynamics to the homologous enzymes AMSH and AMSH-LP. We analyzed stable simulations of the five systems with a maximum RMSD lower than 2.5 Å compared to the respective starting structures. All simulations highlighted the active site flap as a flexible region (Supplemental Figure 5, Figure 10a–e), as indicated by the relative mobility of backbone atoms and side chains of the flap residues. Local backbone B-factors consistently exceeded 0.3 Å^2 for all simulated systems, dihedral entropies were found larger than 94 J/(mol·K) reflecting the high flexibility of the flap region. Supplemental Figure 5 shows the overlay of 20 MD frames for Sst2 with the polypeptide backbone of the region near the active-site flap shown in gray ribbon. The mutated residue, Phe403 in Sst2, is highly mobile both on backbone as well as side chain level (Supplemental Figure 5, and Figure 10b,c). We observe almost free rotation of both phenylalanine and tryptophan at this position. Dimensionless relative side chain flexibilities[68] are 0.92 for Phe403, 0.83 for Trp403, and 0.99 for Ala403, indicating free rotation for the latter residue. The free rotation is paralleled by a loss of molecular interactions with the opposing side of the active-site flap. Hydrogen-bonding of the Trp403 side chain with Asp315, as seen in the static crystal structure, is observed in less than 1% of the snapshots. Additionally, we observe some compensation by hydrogen-bonding between Trp403 and the side chain of Thr316 (3%). In general, all residues at position 403 sample a broad conformational space, including open configurations closely resembling the ubiquitin-bound state. Highest flexibilities are consistently observed for Trp403 among Sst2 mutants using three different metrics capturing dynamics on a global and local scale (Figure 10f–h). The simulated homologous AMSH systems show similar flexibilities in the flap region using all three metrics.

To get further insight into the effects of altered dynamics in Sst2 mutants, we probed Lys48 and Lys11-linked diubiquitin as alternate substrates for the variants studied here. As noted earlier, Sst2, like AMSH and AMSH-LP, is highly selective for Lys63-linked polyubiquitin chains. This selectivity is mainly due to interactions with the proximal ubiquitin, many of which manifest only during the rate-limiting step of the reaction. The flap may contribute to selectivity by virtue of its dynamic properties. If the flap were too flexible, in the extreme case of being completely disordered, it may be reflected in the enzyme losing selectivity. That is, a mutant with a more flexible flap would be expected to show more activity toward Lys48 and Lys11-linked diubiquitin substrates than the wild-type enzyme. On the other hand, a more rigid flap may mean a reduction in the association rate constant for substrate binding. If the latter factor was important, one would expect a loss of activity with substrates regardless of linkage types. We find that the Trp mutant has higher activity with Lys48- and Lys11-linked substrates than the wild-type enzyme, consistent with a loss of selectivity (Figure 11). This observation is in contrast to the Sst2^{F403A} mutant, which shows a reduced activity with all the three substrates tested, perhaps due to the essential contribution of the aromatic ring of the Phe residue to binding of the Lys side chain of the proximal ubiquitin in all the three linkage types studied here. These results, in connection with the molecular dynamics data, indicate that the Trp mutant has a more dynamic flap than the wild-type structure and hence reduced selectivity. Although one cannot rule out other factors behind this reduced selectivity, it seems unlikely that selective

DOI: 10.1021/acs.biochem.5b00631
Biochemistry 2015, 54, 6038–6051

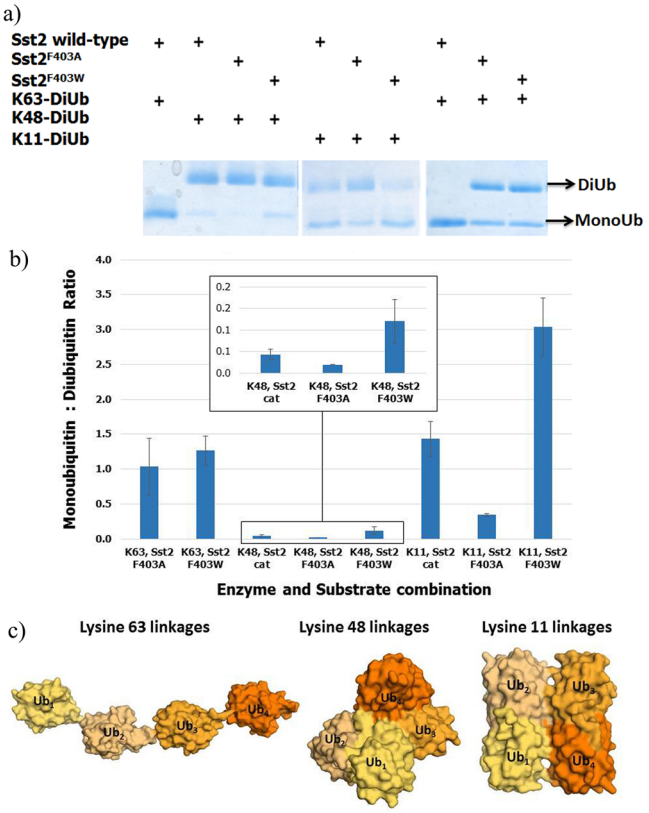

Figure 11. Activity assay conducted by monitoring cleavage of different substrates (Lys63-, Lys48-, and Lys11-linked diubiquitin) by different DUBS (wild-type Sst2, Sst2^{F403A}, and Sst2^{F403W} mutants). (a) SDS-PAGE gel comparing the activity of wild-type Sst2 and its mutants with different substrates. Each reaction mixture contained 250 nM Sst2 catalytic domain or Sst2^{F403A} mutant or Sst2^{F403W} mutant with 20 μM concentrations of Lys63- or Lys48- or Lys11-linked diubiquitin, and each reaction proceeded for 5 h at 20 °C before quenching with 5× SDS-PAGE sample buffers. (b) Representative plot of mono-ubiquitin:diubiquitin ratio as a function of different substrates (Lys63-, Lys48-, and Lys11- linked diubiquitin) and different enzymes (wild-type Sst2, Sst2^{F403A} and Sst2^{F403W} mutants). Bands corresponding to monoubiquitin and diubiquitin were integrated using ImageJ. (c) Different chain morphologies of Lys63-, Lys48-, and Lys11-linked polyubiquitin chain. (PDB ID: 3HM3, 2O6V, and 2XEW, respectively[77−79]).

interactions with the alternative substrates is behind the loss of selectivity observed with the mutant, given that Lys11- and Lys48-linked substrates are structurally quite different (Figure 11c). Structural models of the Sst2 and its Ala and Trp mutants bound to Lys11- and Lys48-linked diubiquitin, generated based on the cocrystal structure of Sst2 bound to Lys63-linked diubiquitin, suggest that active-site flap (Phe403) may impede accurate alignment of these alternative substrates in the active site (see Supplemental Figure 6 and its caption for a description of the method used in model building). Therefore, increased mobility of the flap may result in better accommodation of the scissile peptide bond of these noncognate substrates in the active site of Sst2. However, these models have limited utility since they depict a static snapshot of binding and, more importantly, do not take into account the flexibility of the substrates themselves.

DISCUSSION

It has been widely appreciated that the active sites of enzymes bear flexible loop elements that help in catalysis.[72−75] In the absence of a substrate, such active-site loops are generally disordered, but adopt specific conformations upon substrate binding, often becoming immobilized by forming specific contacts with the substrate. The active-site flap in AMSH is somewhat peculiar in the sense that it oscillates between open and closed states independent of substrate binding. X-ray crystal structures of the DUB domains of both AMSH-LP and Sst2 bound to diubiquitin shows Phe403 collapsed onto the Lys63 side chain of the proximal ubiquitin; however, the flap residues appear to retain their mobility even in the presence of bound substrate or product (indicated by relatively weak electron density enveloping these residues and higher B-factors than internal residues). This is consistent with our observation that mutation of a key conserved residue in the flap (Phe403 in Sst2) does not affect the K_M significantly, implying that the flap residues contribute little to substrate binding in the ground state (to formation of the Michaelis complex). This is particularly clear in the Sst2^{C397A} mutant that is defective for binding to the structural zinc. Loss of the structural zinc causes the active-site flap to become substantially more flexible than the wild-type enzyme, indicated by a significant loss of thermal stability. Yet the mutant does not affect its substrate binding significantly (Table 1). A similar mutant in AMSH-LP (Cys402 to Ser), defective only in k_{cat} like the Sst2^{C397A} mutant, retains nearly the same level of affinity for the ubiquitin product compare to the wild-type enzyme (Table 4 and Supplemental Figure 7), we could not measure K_D for ubiquitin for the Sst2^{C397A} mutant because the mutant could not be isolated in amounts suitable for ITC experiments). However, the loop is especially important for the rate-limiting step, since the Sst2^{C397A} mutant and other mutants studied here are defective primarily in k_{cat}. Immobilization of the active site loop during the key catalytic steps of the reaction, so that Phe403 forms a contact with the Lys63 side chain moiety of the scissile isopeptide bond, imposes a higher entropic penalty as the loop becomes increasingly disordered. This is especially reflected in the significant loss in k_{cat} observed in the Sst2^{C397A} mutant, whose active site loop has become quite flexible due to loss of the structural zinc.

Our results seem to indicate that the flexibility of active-site flaps is precisely tuned to be in step with catalytic events. It is possible that, while keeping the catalytic mechanism conserved, evolution may fine-tune flexibility for selectivity.[71] The flexibility of the flap in Sst2 appears to be controlled by (1) the structural zinc in the insertion 2 component of AMSH and AMSH-like enzymes and (2) by an additional interaction of the flap residue Phe403, which makes a contact with the Asp side chain across the active-site cleft. This may be why the Phe403 residue and Asp315 are strictly conserved among AMSH-like JAMM proteases. The contact distance between Phe403 and Asp315 is approximately 4.0 Å in the crystal structures of AMSH, AMSH-LP and Sst2, a distance indicative of a stabilizing interaction termed anion-π interaction.[70,76] A recent analysis of the PDB reveals a widespread presence of such contacts, indicating a role of anion-π interactions in protein stability. Perhaps the loss of the anion-π interaction in the Sst2^{F403A} mutant leading to increased loop flexibility, and thus an increased entropic penalty, contributes to the loss of activity observed with the Ala mutant. Mutation of the Asp residue to

DOI: 10.1021/acs.biochem.5b00631
Biochemistry 2015, 54, 6038−6051

Asn indeed results in a defective enzyme, by a nearly 7-fold loss in activity, primarily due to a reduction in k_{cat} (Table 1). It is possible that this loss of activity reflects loss of the anion-π interaction. Loss of this interaction might have the effect of making the flap more dynamic and is expected to produce an effect in line with the Trp mutant. However, a closer inspection of the diubiquitin-bound crystal structure reveals that the Asp residue is 4 Å from amino-group of Met1 of the proximal ubiquitin of the diubiquitin substrate, a distance range in which there maybe appreciable electrostatic attraction between the carboxylate and the amino group (likely protonated at the nearly neutral pH of the assay buffer). The loss of activity in the Asn mutant might also reflect, at least to a degree, a loss of the columbic attraction.

Contrary to our expectation, it appears that the active-site flap in the Trp mutant has higher flexibility than the wild-type enzyme. Since our crystal structure shows the Trp side chain is identically positioned to interact with the substrate as the Phe403 residue in the wild-type enzyme, we propose that the loss of activity in the mutant, due to decreased k_{cat}, is suggestive of altered dynamics and is supported by our molecular dynamics data. However, we cannot rule out other factors contributing to impaired catalysis seen here, such as the precise orientation of the Trp side chain during the catalytic steps relative to the Phe side chain in the wild-type enzyme. Some evidence of this higher flexibility can be seen in B-factors of the flap in the crystal structure of the mutant. Despite the flap being somewhat immobilized by the crystallographic contacts (Supplemental Figure 4), the elevated B-factors of these residues are indicative of the loop's mobility in solution (Supplemental Table 1). Molecular dynamics simulations clearly indicate that the active-site flap of Sst2 is quite mobile and samples various conformations on the microsecond time-scale. The Sst2^{F403W} mutant shows the highest mobility on three different flexibility metrics, thus underlining a gain in mobility in this mutant. An additional but indirect evidence of higher flexibility can be the observation that Lys11- and Lys48-linked diubiquitin substrates are cleaved more readily by the mutants than the wild-type enzyme. It is possible that this reflects enhanced flexibility of the flap, giving rise to a more open active-site cleft. This more open active-site cleft can better accommodate alternative diubiquitin substrates, while the wild-type enzyme is more selective for Lys63 linkage due to a strict steric requirement imposed by the active-site flap. While not contributing to substrate binding per se, higher flexibility of the flap could mean a higher probability that it spends more time away from the active-site, which could mean the active-site cleft is somewhat more exposed than when the flap has less flexibility. This "open" active-site may therefore pose less stringency on the precise nature of the substrate. That is, the enzyme with a more flexible flap may be less selective. The implication of this observation could be that the flap in AMSH-like enzyme might have evolved to increase selectivity by discriminating against other types of polyubiquitin chain substrates due to diminished flexibility.

■ ASSOCIATED CONTENT

Supporting Information

The Supporting Information is available free of charge on the ACS Publications website at DOI: 10.1021/acs.biochem.5b00631.

Tables of comparison of B-factors between internal residues and flap residues; estimation of secondary structures from CD spectra. Supplemental figures of the structure of the catalytic domain of Sst2 wild-type and its mutants Sst2^{F403A} and Sst2^{F403W}; SDS-PAGE gel of reactions; electron density map; crystallographic contacts of subunits of Sst2^{F403W}; overlay of the Sst2 crystal structure; models of Sst2 wild-type and its mutants Sst2^{F403W} and Sst2^{F403A} bound to Lys11- and Lys48-linked diubiquitin; determination of thermodynamic parameters for AMSH-LP and AMSH-LP^{C402S}. Model building methods (PDF)

Accession Codes

Coordinates and structure factors have been deposited in the PDB with accession numbers 4ZD5 (Sst2^{F403A}), 4ZD4 (Sst2^{F403W}), 4ZFR (Sst2^{F403A}-Ub) and 4ZFT (Sst2^{F403W}-Ub).

■ AUTHOR INFORMATION

Corresponding Author

*Phone: (765) 494-5478. Fax: (765) 494-0239. E-mail: cdas@purdue.edu.

Present Addresses

‡Department of Molecular Biophysics and Biochemistry, Yale University, 266 Whitney Avenue, New Haven, Connecticut, 06520, United States.

‖Institute of General, Inorganic, and Theoretical Chemistry, University of Innsbruck, Innrain 82, 6020, Innsbruck, Austria.

Author Contributions

#A.N.B. and R.K.S. contributed equally.

Funding

This research was funded by the National Institutes of Health (2R01GM103401 to C.D.).

Notes

The authors declare no competing financial interest.

■ ACKNOWLEDGMENTS

We are grateful to our hosts Sudhir Pothineni and Sioan Zohar at the GM/CA CAT beamline 23-ID-B at the Advanced Photon Source, Argonne National Laboratory. Use of the Advanced Photon Source, an Office of Science User Facility operated for the U.S. Department of Energy (DOE) Office of Science by Argonne National Laboratory, was supported by the U.S. DOE under Contract No. DE-AC02-06CH11357.

■ ABBREVIATIONS

DUB, deubiquitinating enzyme; JAMMs, JAB1/MPN/MOV34 metalloenzymes; AMSH, associated molecule with the SH3 domain of STAM; AMSH-LP, AMSH-like protein; Sst2, AMSH-like protease Sst2; ESCRT, endosomal sorting complexes required for transport; GST, glutathione-*S*-transferase; IPTG, isopropyl-β-D-thiogalactoside; SEC, size exclusion chromatography; ITC, isothermal titration calorimetry; CD, circular dichroism; PDB, Protein Data Bank; PEG, polyethylene glycol; HEPES, 2-[4-(2-hydroxyethyl)piperzan-1-yl]-ethanesulfonic acid

■ REFERENCES

(1) Hershko, A., and Ciechanover, A. (1998) The ubiquitin system. *Annu. Rev. Biochem. 67*, 425−479.

(2) Xu, G., and Jaffrey, S. R. (2011) The new landscape of protein ubiquitination. *Nat. Biotechnol. 29*, 1098−1100.

DOI: 10.1021/acs.biochem.5b00631
Biochemistry 2015, 54, 6038−6051

(3) Finley, D., Ciechanover, A., and Varshavsky, A. (2004) Ubiquitin as a central cellular regulator. *Cell 116*, S29−32.
(4) Varshavsky, A. (1997) The ubiquitin system. *Trends Biochem. Sci. 22*, 383−387.
(5) Haglund, K., and Dikic, I. (2005) Ubiquitylation and cell signaling. *EMBO J. 24*, 3353−3359.
(6) Ikeda, F., and Dikic, I. (2008) Atypical ubiquitin chains: new molecular signals. 'Protein Modifications: Beyond the Usual Suspects' review series. *EMBO Rep. 9*, 536−542.
(7) Pickart, C. M. (2000) Ubiquitin in chains. *Trends Biochem. Sci. 25*, 544−548.
(8) Schulman, B. A. (2011) Twists and turns in ubiquitin-like protein conjugation cascades. *Protein Sci. 20*, 1941−1954.
(9) Komander, D., and Rape, M. (2012) The ubiquitin code. *Annu. Rev. Biochem. 81*, 203−229.
(10) Fushman, D., and Wilkinson, K. D. (2011) Structure and recognition of polyubiquitin chains of different lengths and linkage. *F1000 Biol. Rep 3*, 26.
(11) Chen, Z. J., and Sun, L. J. (2009) Nonproteolytic functions of ubiquitin in cell signaling. *Mol. Cell 33*, 275−286.
(12) Kulathu, Y., and Komander, D. (2012) Atypical ubiquitylation - the unexplored world of polyubiquitin beyond Lys48 and Lys63 linkages. *Nat. Rev. Mol. Cell Biol. 13*, 508−523.
(13) Amerik, A. Y., and Hochstrasser, M. (2004) Mechanism and function of deubiquitinating enzymes. *Biochim. Biophys. Acta, Mol. Cell Res. 1695*, 189−207.
(14) Love, K. R., Catic, A., Schlieker, C., and Ploegh, H. L. (2007) Mechanisms, biology and inhibitors of deubiquitinating enzymes. *Nat. Chem. Biol. 3*, 697−705.
(15) Wilkinson, K. D. (1997) Regulation of ubiquitin-dependent processes by deubiquitinating enzymes. *FASEB J. 11*, 1245−1256.
(16) Nijman, S. M., Luna-Vargas, M. P., Velds, A., Brummelkamp, T. R., Dirac, A. M., Sixma, T. K., and Bernards, R. (2005) A genomic and functional inventory of deubiquitinating enzymes. *Cell 123*, 773−786.
(17) Hussain, S., Zhang, Y., and Galardy, P. J. (2009) DUBs and cancer: the role of deubiquitinating enzymes as oncogenes, non-oncogenes and tumor suppressors. *Cell Cycle 8*, 1688−1697.
(18) Atkin, G., and Paulson, H. (2014) Ubiquitin pathways in neurodegenerative disease. *Front. Mol. Neurosci. 7*, 63.
(19) Todi, S. V., and Paulson, H. L. (2011) Balancing act: deubiquitinating enzymes in the nervous system. *Trends Neurosci. 34*, 370−382.
(20) Das, C., Hoang, Q. Q., Kreinbring, C. A., Luchansky, S. J., Meray, R. K., Ray, S. S., Lansbury, P. T., Ringe, D., and Petsko, G. A. (2006) Structural basis for conformational plasticity of the Parkinson's disease-associated ubiquitin hydrolase UCH-L1. *Proc. Natl. Acad. Sci. U. S. A. 103*, 4675−4680.
(21) Komander, D., Clague, M. J., and Urbe, S. (2009) Breaking the chains: structure and function of the deubiquitinases. *Nat. Rev. Mol. Cell Biol. 10*, 550−563.
(22) Komander, D. (2010) Mechanism, specificity and structure of the deubiquitinases. *Subcell. Biochem. 54*, 69−87.
(23) Wilkinson, K. D. (2009) DUBs at a glance. *J. Cell Sci. 122*, 2325−2329.
(24) Verma, R., Aravind, L., Oania, R., McDonald, W. H., Yates, J. R., III, Koonin, E. V., and Deshaies, R. J. (2002) Role of Rpn 11 metalloprotease in deubiquitination and degradation by the 26S proteasome. *Science 298*, 611−615.
(25) Echalier, A., Pan, Y. B., Birol, M., Tavernier, N., Pintard, L., Hoh, F., Ebel, C., Galophe, N., Claret, F. X., and Dumas, C. (2013) Insights into the regulation of the human COP9 signalosome catalytic subunit, CSN5/Jab1. *Proc. Natl. Acad. Sci. U. S. A. 110*, 1273−1278.
(26) Sobhian, B., Shao, G., Lilli, D. R., Culhane, A. C., Moreau, L. A., Xia, B., Livingston, D. M., and Greenberg, R. A. (2007) RAP80 targets BRCA1 to specific ubiquitin structures at DNA damage sites. *Science 316*, 1198−1202.
(27) Guterman, A., and Glickman, M. H. (2004) Deubiquitinating enzymes are IN/(trinsic to proteasome function). *Curr. Protein Pept. Sci. 5*, 201−211.
(28) Yao, T., and Cohen, R. E. (2002) cryptic protease couples deubiquitination and degradation by the proteasome. *Nature 419*, 403−407.
(29) Lingaraju, G. M., Bunker, R. D., Cavadini, S., Hess, D., Hassiepen, U., Renatus, M., Fischer, E. S., and Thoma, N. H. (2014) Crystal structure of the human COP9 signalosome. *Nature 512*, 161−165.
(30) Kyuuma, M., Kikuchi, K., Kojima, K., Sugawara, Y., Sato, M., Mano, N., Goto, J., Takeshita, T., Yamamoto, A., Sugamura, K., and Tanaka, N. (2006) AMSH, an ESCRT-III associated enzyme, deubiquitinates cargo on MVB/late endosomes. *Cell Struct. Funct. 31*, 159−172.
(31) Birol, M., and Echalier, A. (2014) Structure and function of MPN (Mpr1/Pad1 N-terminal) domain-containing proteins. *Curr. Protein Pept. Sci. 15*, 504−517.
(32) Sato, Y., Yoshikawa, A., Yamagata, A., Mimura, H., Yamashita, M., Ookata, K., Nureki, O., Iwai, K., Komada, M., and Fukai, S. (2008) Structural basis for specific cleavage of Lys 63-linked polyubiquitin chains. *Nature 455*, 358−U319.
(33) Raiborg, C., and Stenmark, H. (2009) The ESCRT machinery in endosomal sorting of ubiquitylated membrane proteins. *Nature 458*, 445−452.
(34) Clague, M. J., and Urbe, S. (2006) Endocytosis: the DUB version. *Trends Cell Biol. 16*, 551−559.
(35) McCullough, J., Clague, M. J., and Urbe, S. (2004) AMSH is an endosome-associated ubiquitin isopeptidase. *J. Cell Biol. 166*, 487−492.
(36) Saksena, S., Sun, J., Chu, T., and Emr, S. D. (2007) ESCRTing proteins in the endocytic pathway. *Trends Biochem. Sci. 32*, 561−573.
(37) Wollert, T., Wunder, C., Lippincott-Schwartz, J., and Hurley, J. H. (2009) Membrane scission by the ESCRT-III complex. *Nature 458*, 172−U172.
(38) Wollert, T., and Hurley, J. H. (2010) Molecular mechanism of multivesicular body biogenesis by ESCRT complexes. *Nature 464*, 864−869.
(39) Henne, W. M., Buchkovich, N. J., and Emr, S. D. (2011) The ESCRT pathway. *Dev. Cell 21*, 77−91.
(40) Davies, C. W., Paul, L. N., Kim, M. I., and Das, C. (2011) Structural and thermodynamic comparison of the catalytic domain of AMSH and AMSH-LP: nearly identical fold but different stability. *J. Mol. Biol. 413*, 416−429.
(41) Solomons, J., Sabin, C., Poudevigne, E., Usami, Y., Hulsik, D. L., Macheboeuf, P., Hartlieb, B., Gottlinger, H., and Weissenhorn, W. (2011) Structural basis for ESCRT-III CHMP3 recruitment of AMSH. *Structure 19*, 1149−1159.
(42) Kim, M. S., Kim, J. A., Song, H. K., and Jeon, H. (2006) STAM-AMSH interaction facilitates the deubiquitination activity in the C-terminal AMSH. *Biochem. Biophys. Res. Commun. 351*, 612−618.
(43) McCullough, J., Row, P. E., Lorenzo, O., Doherty, M., Beynon, R., Clague, M. J., and Urbe, S. (2006) Activation of the endosome-associated ubiquitin isopeptidase AMSH by STAM, a component of the multivesicular body-sorting machinery. *Curr. Biol. 16*, 160−165.
(44) Davies, C. W., Paul, L. N., and Das, C. (2013) Mechanism of recruitment and activation of the endosome-associated deubiquitinase AMSH. *Biochemistry 52*, 7818−7829.
(45) Carter, M. T., and Boycott, K. M. (2011) Microcephaly-Capillary Malformation Syndrome: A Story of Rapid Emergence of a New Recognizable Entity. *Am. J. Med. Genet., Part A 155*, 2078−2079.
(46) McDonell, L. M., Mirzaa, G. M., Alcantara, D., Schwartzentruber, J., Carter, M. T., Lee, L. J., Clericuzio, C. L., Graham, J. M., Morris-Rosendahl, D. J., Polster, T., Acsadi, G., Townshend, S., Williams, S., Halbert, A., Isidor, B., David, A., Smyser, C. D., Paciorkowski, A. R., Willing, M., Woulfe, J., Das, S., Beaulieu, C. L., Marcadier, J., Geraghty, M. T., Frey, B. J., Majewski, J., Bulman, D. E., Dobyns, W. B., O'Driscoll, M., Boycott, K. M., and Consortium, F. C. (2013) Mutations in STAMBP, encoding a deubiquitinating enzyme, cause microcephaly-capillary malformation syndrome. *Nat. Genet. 45*, 556−562.
(47) Shrestha, R. K., Ronau, J. A., Davies, C. W., Guenette, R. G., Strieter, E. R., Paul, L. N., and Das, C. (2014) Insights into the

DOI: 10.1021/acs.biochem.5b00631
Biochemistry 2015, 54, 6038−6051

Mechanism of Deubiquitination by JAMM Deubiquitinases from Cocrystal Structures of the Enzyme with the Substrate and Product. *Biochemistry 53*, 3199−3217.
(48) Otwinowski, Z., and Minor, W. (1997) Processing of X-ray diffraction data collected in oscillation mode. *Methods Enzymol. 276*, 307−326.
(49) Lebedev, A. A., Vagin, A. A., and Murshudov, G. N. (2008) Model preparation in MOLREP and examples of model improvement using X-ray data. *Acta Crystallogr., Sect. D: Biol. Crystallogr. 64*, 33−39.
(50) Collaborative Computational Project, Number 4 (1994) The Ccp4 Suite - Programs for Protein Crystallography. *Acta Crystallogr., Sect. D: Biol. Crystallogr. 50*, 760−763.
(51) Emsley, P., Lohkamp, B., Scott, W. G., and Cowtan, K. (2010) Features and development of Coot. *Acta Crystallogr., Sect. D: Biol. Crystallogr. 66*, 486−501.
(52) Murshudov, G. N., Skubak, P., Lebedev, A. A., Pannu, N. S., Steiner, R. A., Nicholls, R. A., Winn, M. D., Long, F., and Vagin, A. A. (2011) REFMAC5 for the refinement of macromolecular crystal structures. *Acta Crystallogr., Sect. D: Biol. Crystallogr. 67*, 355−367.
(53) Adams, P. D., Grosse-Kunstleve, R. W., Hung, L. W., Ioerger, T. R., McCoy, A. J., Moriarty, N. W., Read, R. J., Sacchettini, J. C., Sauter, N. K., and Terwilliger, T. C. (2002) PHENIX: building new software for automated crystallographic structure determination. *Acta Crystallogr., Sect. D: Biol. Crystallogr. 58*, 1948−1954.
(54) Painter, J., and Merritt, E. A. (2006) Optimal description of a protein structure in terms of multiple groups undergoing TLS motion. *Acta Crystallogr., Sect. D: Biol. Crystallogr. 62*, 439−450.
(55) *The PyMOL Molecular Graphics System*, Version 1.7.0.0, Schrödinger, LLC, München.
(56) Schneider, C. A., Rasband, W. S., and Eliceiri, K. W. (2012) NIH Image to ImageJ: 25 years of image analysis. *Nat. Methods 9*, 671−675.
(57) Perez-Iratxeta, C. a., and Andrade-Navarro, M. A. (2008) K2D2: estimation of protein secondary structure from circular dichroism spectra. *BMC Struct. Biol. 8*, 25.
(58) Louis-Jeune, C., Andrade-Navarro, M. A., and Perez-Iratxeta, C. (2012) Prediction of protein secondary structure from circular dichroism using theoretically derived spectra. *Proteins: Struct., Funct., Genet. 80*, 374−381.
(59) Keller, S., Vargas, C., Zhao, H. Y., Piszczek, G., Brautigam, C. A., and Schuck, P. (2012) High-Precision Isothermal Titration Calorimetry with Automated Peak-Shape Analysis. *Anal. Chem. 84*, 5066−5073.
(60) Houtman, J. C. D., Brown, P. H., Bowden, B., Yamaguchi, H., Appella, E., Samelson, L. E., and Schuck, P. (2007) Studying multisite binary and ternary protein interactions by global analysis of isothermal titration calorimetry data in SEDPHAT: Application to adaptor protein complexes in cell signaling. *Protein Sci. 16*, 30−42.
(61) Case, D. A., Berryman, J. T., Betz, R. M., Cerutti, D. S., Cheatham, III, T. E., Darden, T. A., Duke, R. E., Giese, T. J.,Gohlke, H., Goetz, H. W., Homeyer, N., Izadi, S., Janowski, P., Kaus, J., Kovalenko, A., Lee, T. S., LeGrand, S., Li, P., Luchko, T., Luo, R., Madej, B., Merz, K. M., Monard, G., Needham, P.,Nguyen, H., Nguyen, H. T., Omelyan, I., Onufriev, A., Roe, D. R., Roitberg, A., Salomon-Ferrer, R., Simmerling, C. L., Smith, W., Swails, J., Walker, R. C., Wang, J., Wolf, R. M., Wu, X., York, D. M., and Kollman, P. A. (2015) *AMBER 2015*, University of California, San Francisco.
(62) Labute, P. (2009) Protonate3D: assignment of ionization states and hydrogen coordinates to macromolecular structures. *Proteins: Struct., Funct., Genet. 75*, 187−205.
(63) Lindorff-Larsen, K., Piana, S., Palmo, K., Maragakis, P., Klepeis, J. L., Dror, R. O., and Shaw, D. E. (2010) Improved side-chain torsion potentials for the Amber ff99SB protein force field. *Proteins: Struct., Funct., Genet. 78*, 1950−1958.
(64) Jorgensen, W. L., Chandrasekhar, J., Madura, J. D., Impey, R. W., and Klein, M. L. (1983) Comparison of simple potential functions for simulating liquid water. *J. Chem. Phys. 79*, 926.
(65) Vanquelef, E., Simon, S., Marquant, G., Garcia, E., Klimerak, G., Delepine, J. C., Cieplak, P., and Dupradeau, F. Y. (2011) R.E.D. Server: a web service for deriving RESP and ESP charges and building force field libraries for new molecules and molecular fragments. *Nucleic Acids Res. 39*, W511−517.
(66) Fuchs, J. E., Huber, R. G., von Grafenstein, S., Wallnoefer, H. G., Spitzer, G. M., Fuchs, D., and Liedl, K. R. (2012) Dynamic regulation of phenylalanine hydroxylase by simulated redox manipulation. *PLoS One 7*, e53005.
(67) Roe, D. R., and Cheatham, T. E., III (2013) PTRAJ and CPPTRAJ: Software for Processing and Analysis of Molecular Dynamics Trajectory Data. *J. Chem. Theory Comput. 9*, 3084−3095.
(68) Fuchs, J. E., Waldner, B. J., Huber, R. G., von Grafenstein, S., Kramer, C., and Liedl, K. R. (2015) Independent Metrics for Protein Backbone and Side-Chain Flexibility: Time Scales and Effects of Ligand Binding. *J. Chem. Theory Comput. 11*, 851−860.
(69) Huber, R. G., Eibl, C., and Fuchs, J. E. (2015) Intrinsic flexibility of NLRP pyrin domains is a key factor in their conformational dynamics, fold stability, and dimerization. *Protein Sci. 24*, 174−181.
(70) Philip, V., Harris, J., Adams, R., Nguyen, D., Spiers, J., Baudry, J., Howell, E. E., and Hinde, R. J. (2011) A survey of aspartate-phenylalanine and glutamate-phenylalanine interactions in the protein data bank: searching for anion-pi pairs. *Biochemistry 50*, 2939−2950.
(71) Fuchs, J. E., von Grafenstein, S., Huber, R. G., Wallnoefer, H. G., and Liedl, K. R. (2014) Specificity of a protein-protein interface: local dynamics direct substrate recognition of effector caspases. *Proteins: Struct., Funct., Genet. 82*, 546−555.
(72) Aung, H. P., Bocola, M., Schleper, S., and Rohm, K. H. (2000) Dynamics of a mobile loop at the active site of Escherichia coli asparaginase. *Biochim. Biophys. Acta, Protein Struct. Mol. Enzymol. 1481*, 349−359.
(73) Aglietti, R. A., Floor, S. N., McClendon, C. L., Jacobson, M. P., and Gross, J. D. (2013) Active site conformational dynamics are coupled to catalysis in the mRNA decapping enzyme Dcp2. *Structure 21*, 1571−1580.
(74) McElheny, D., Schnell, J. R., Lansing, J. C., Dyson, H. J., and Wright, P. E. (2005) Defining the role of active-site loop fluctuations in dihydrofolate reductase catalysis. *Proc. Natl. Acad. Sci. U. S. A. 102*, 5032−5037.
(75) Schwartz, S. D., and Schramm, V. L. (2009) Enzymatic transition states and dynamic motion in barrier crossing. *Nat. Chem. Biol. 5*, 551−558.
(76) Jackson, M. R., Beahm, R., Duvvuru, S., Narasimhan, C., Wu, J., Wang, H., Philip, V. M., Hinde, R. J., and Howell, E. E. (2007) A Preference for Edgewise Interactions between Aromatic Rings and Carboxylate Anions: The Biological Relevance of Anion-Quadrupole Interactions. *J. Phys. Chem. B 111*, 8242−8249.
(77) Datta, A. B., Hura, G. L., and Wolberger, C. (2009) The structure and conformation of Lys63-linked tetraubiquitin. *J. Mol. Biol. 392*, 1117−1124.
(78) Eddins, M. J., Varadan, R., Fushman, D., Pickart, C. M., and Wolberger, C. (2007) Crystal structure and solution NMR studies of Lys48-linked tetraubiquitin at neutral pH. *J. Mol. Biol. 367*, 204−211.
(79) Bremm, A., Freund, S. M., and Komander, D. (2010) Lys11-linked ubiquitin chains adopt compact conformations and are preferentially hydrolyzed by the deubiquitinase Cezanne. *Nat. Struct. Mol. Biol. 17*, 939−947.

DOI: 10.1021/acs.biochem.5b00631
Biochemistry 2015, 54, 6038−6051